Oil & Gas Science and Technology – Rev. IFP Energies nouvelles **75**, 87 (2020)

https://doi.org/10.2516/ogst/2020072

Available online at:
ogst.ifpenergiesnouvelles.fr

REGULAR ARTICLE OPEN ACCESS

Experimental study of *in-situ* W/O emulsification during the injection of $MgSO_4$ and Na_2CO_3 solutions in a glass micromodel

Sepideh Palizdan[1], Hossein Doryani[2], Masoud Riazi[1,*], and Mohammad Reza Malayeri[1,3]

[1] Enhanced Oil Recovery Research Centre, Department of Petroleum Engineering, School of Chemical and Petroleum Eng., Shiraz University, Shiraz 71946 85115, Iran
[2] Institute of GeoEnergy Engineering, School of Energy, Geoscience, Infrastructure and Society, Heriot-Watt University, Edinburgh, UK
[3] Institut für Verfahrenstechnik und Umwelttechnik (IVU), Technische Universität Dresden, 01062 Dresden, Germany

Received: 11 May 2020 / Accepted: 7 September 2020

Abstract. *In-situ* emulsification of injected brines of various types is gaining increased attention for the purpose of enhanced oil recovery. The present experimental study aims at evaluating the impact of injecting various solutions of Na_2CO_3 and $MgSO_4$ at different flow rates resembling those in the reservoir and near wellbore using a glass micromodel with different permeability regions. Emulsification process was visualized through the injection of deionized water and different brines at different flow rates. The experimental results showed that the extent of emulsions produced in the vicinity of the micromodel exit was profoundly higher than those at the entrance of the micromodel. The injection of Na_2CO_3 brine after deionized water caused the impact of emulsification process more efficiently for attaining higher oil recovery than that for the $MgSO_4$ brine. For instance, the injection of $MgSO_4$ solution after water flooding increased oil recovery only up to 1%, while the equivalent figure for Na_2CO_3 was 28%. It was also found that lower flow rate of injection would cause the displacement front to be broadened since the injected fluid had more time to interact with the oil phase. Finally, lower injection flow rate reduced the viscous force of the displacing fluid which led to lesser occurrence of viscous fingering phenomenon.

1 Introduction

Several problems may arise during the production from heavy oil reservoirs including considerably high viscosity and precipitation/deposition of asphaltene. Generally speaking, only 3–10% of *in-situ* oil in heavy oil reservoirs is produced by natural reservoir forces (Pei *et al.*, 2013a). As a result, the investigation of Enhanced Oil Recovery (EOR) from heavy oil reservoirs is of prime importance. Most of the proposed methods for increasing oil recovery are based on oil viscosity reduction or decreasing the mobility ratio of the displacing fluid to the displaced fluid (Sun *et al.*, 2019). Thermal enhanced oil recovery methods can also be potentially useful which can profoundly increase the oil recovery. This is due to considerable reduction in oil viscosity, its mobility in porous media can then be increased substantially, thus, resulting in an enhanced oil recovery. The main problem with this method, though, is the heat loss which can take place in deep and low thickness reservoirs (Pei *et al.*, 2013b; Pu *et al.*, 2019; Thomas, 2008).

Conventional water flooding is another approach which would usually come with a lower price tag. However, conventional water flooding would leave considerable amount of oil unrecovered. This is mainly due to the low microscopic (pore-level) and macroscopic sweep efficiency (volumetric) of this method. Low sweep efficiency and pore size displacement efficiency are due to the undesirable mobility ratio and high Interfacial Tension (IFT) existing between fluids in the porous media, respectively. Oil trapping in pore spaces of the rock is controlled by the active forces in porous media, namely capillary and viscous forces. Hence, capillary number which, by definition, is the ratio of viscous to capillary forces would serve as a controlling factor in the displacement process (Bryan and Kantzas 2007; Bryan *et al.*, 2008; Mai and Kantzas 2009; Sabooniha *et al.*, 2019). Fluid velocity is also a key parameter for the fluid flow in porous media, especially the transport of the emulsion phase. The magnitude of the velocity would be a prevailing factor for the behavior of the dispersed droplets or their entrapment, break or movement in porous media (Shang *et al.*, 2019; Soo and Radke, 1984).

Emulsification has long been considered as a viable option for EOR purposes. Various effects contribute to the emulsion stability including the presence of heavy polar particles in the crude oil like asphaltene, solid particles, pressure, temperature, the size distribution of the droplets,

* Corresponding author: mriazi@shirazu.ac.ir

pH of the brine and its composition (Akizuki *et al.*, 2014). Ions of higher valence react with asphaltene and as a consequence, asphaltene molecule would go to the interface of water/oil (Shahsavani *et al.*, 2019). Also, the adsorption of asphaltene at the interface of water/oil increases with pressure. The reason lies in the fact that the adsorption is amplified by increasing the pressure (Kazemzadeh *et al.*, 2019). Alkaline injection can improve oil recovery before the precipitation of asphaltene and do not have any significant impacts after asphaltene precipitation (Doryani *et al.*, 2017). Regarding the concepts of capillary number and mobility ratio, emulsification would increase both microscopic and macroscopic sweep efficiencies, respectively (Karambeigi *et al.*, 2015; Umar *et al.*, 2018). Considerable decrease of the interfacial tension between the fluids and enhanced favorable mobility ratio would result in higher microscopic and macroscopic oil recovery (Liu *et al.*, 2006; Saha *et al.*, 2018). Accordingly, *in-situ* emulsification, which is the product of chemical reaction between the two displaced and displacing fluids in the reservoirs due to the injection of different chemicals including surfactant and alkalis, has been the subject of many recent studies (Alvarado, 1979; Kumar *et al.*, 2010; Mehranfar and Ghazanfari, 2014; Taiwo *et al.*, 2016).

W/O emulsions can boost the oil recovery by two probable mechanisms, namely, (i) oil droplets can block the pore spaces and make the fluid flow path to be diverted and (ii) dispersed oil droplets can be produced along with the water phase. As for the W/O emulsions, they could though have remarkably higher viscosity. Emulsion viscous phase can barricade the flow in permeable water saturated channels, resulting in the production of oil from different channels with un-swept residual oil (Farias *et al.*, 2012; Schmidt *et al.*, 1984). According to the concept of ganglia dynamics, as emulsion droplets are trapped in pore spaces, critical capillary force would be needed to move them. Critical capillary force is the minimum force which is needed to displace the oil phase and increased capillary force can cause the production of the continuous phase (Youssef *et al.*, 2014).

Alkaline injection can also improve the oil recovery through the formation of emulsions. The potential is particularly high for enhanced recovery from heavy acidic oil reservoirs. This is mainly because alkali agents can react with the acidic components of crude oil and decrease the interfacial tension. Other prevailing mechanisms which are considered to be important in alkaline injection include wettability alteration, emulsification with entrainment, and emulsification with entrapment (Alvarado, 1979; Dong *et al.*, 2007; Farias *et al.*, 2012; Kumar *et al.*, 2010; Mehranfar and Ghazanfari, 2014; Schmidt *et al.*, 1984; Taiwo *et al.*, 2016; Youssef *et al.*, 2014).

As for the impact of fluid mechanics in porous media, Soot and Radke (1984) quantitatively investigated the possible effects of the velocity on the transport of emulsions in porous media regarding deep bed filtration. They concluded that the velocity would be influential in straining capture regime in the capillary number of 10^{-4}. Rudin *et al.* (1994) studied the effects of adding surfactants and emulsification in a system containing alkali and acidic crude oil. They found that the addition of surfactants to the solution of NaCl brine and alkaline would meaningfully reduce the interfacial tension, resulting in spontaneous emulsification. Sheng (2010, 2015) reported that in chemical flooding, when the volume of one phase is higher than the other phase, then it can be considered as continuous phase. As a result, oil-water ratio is a determining factor which would then influence the type of the emulsion. Moreover, it was pointed out that in the systems containing heavy oils, water droplets would collide less than oil droplets since the oil viscosity is considerably higher than that of water. Thus, in such systems water in oil emulsions are more common than oil in water emulsions.

Bryan and Kantzas (2007) experimentally showed that the injection of alkaline-surfactant solutions would form emulsions mainly due to the profound decrease of the interfacial tension. In this process, emulsification enhances the oil recovery through pore flow restriction, fluid flow diversion and decreased mobility ratio between water and heavy oil. Experimental and simulation results of the study conducted by Wang and Dong (2009) and Wang *et al.* (2010) showed that alkaline injection can cause in-situ emulsification and thus improves oil recovery process in sand-packs. Farias *et al.* (2012) investigated the application of W/O emulsions in enhanced heavy oil recovery. *In-situ* residual oil was used as the hydrocarbon phase of the emulsion. They compared the effectiveness of the injection of emulsion, surfactant and water in terms of increasing oil recovery. The results demonstrated that surfactant and emulsion injection would profoundly increase the oil recovery. In addition, the emulsion phase was capable of decreasing the ratio of water and oil accumulation in comparison with the injection of water. By the use of micromodel experiments, Rezaei and Firoozabadi (2014) figured out that water in oil emulsion droplets can block the pore throat and make the fluids to be transported in other flow passages. They reported that straining and interception mechanisms were responsible for such phenomena. The experimental study was done by Feng *et al.* (2018) shows that oil recovery factor can be improved during Fine Emulsion (FE) flooding by reduction of IFT and strong emulsifying performance. Their experiments indicate that there are two main mechanisms which can happen through injection in micromodel, including performance control of the W/O emulsion and emulsification carrying-on.

As for the impact of asphaltene on emulsification, Poteau *et al.* (2005) showed that the surface charge of asphaltene could be changed in different pH values of the environment, here oil/water mixture. Therefore, the phase behavior of emulsion formation during the injection of water-based methods can have an opposite effect on the oil recovery. Moreover, during the use of water-based methods, if the asphaltene in the oil is unstable, it can then lead to the formation of emulsions. It should be pointed out nevertheless that there have been not enough experimental studies concerning the *in-situ* emulsification process at near wellbore region of heavy oil petroleum reservoirs. In this study, a layered glass micromodel was designed and constructed using a geometrical reservoirs pattern. Mechanisms contributing to the emulsification processes at near wellbore

Table 1. SARA analysis of the investigated crude oil.

Saturates (wt.%)	Aromatic (wt.%)	Asphaltene (wt.%)	Resin (wt.%)
43.5	35.6	8	12.9

Table 2. CHNS analysis of the extracted asphaltene (wt.%).

Element	C	H	N	S	O
Weight percentage	76.16	7.23	0.68	8.3	7.63

region where the fluid velocity is substantially high were then investigated. Layered glass micromodels facilitate the investigation of the effect of permeability on such processes. Mechanisms for production due to the formation of emulsions are presented visually. Also, a comparison between the impacts of $MgSO_4$ and Na_2CO_3 in terms of the extent of emulsification is presented visually in this study.

2 Materials and methodology

2.1 Crude oil and brine properties

The crude oil, investigated in this study, originates from one of the southern oil fields in Iran with an API and density of 27.9 and 0.934 gr/cm^3, respectively. The SARA (Saturate, Aromatic, Resin and Asphaltene) index of the crude oil is presented in Table 1. As it was mentioned, pH is a critical factor influencing the surface charge of asphaltene; therefore, $MgSO_4$ with acidic and Na_2CO_3 with basic pH values were selected. These salts were also of *Merck* grade with the purity of 99%.

2.2 CHNS analysis

CHNS-O analysis was performed using FlashEA (1112 series) based on the ASTM D-5291 method for determination of carbon, hydrogen, nitrogen and oxygen contents of the sample. The carrier gas used in this measurement was helium. Table 2 presents the results of CHNS analysis of asphaltene, according to the results obtained by Chilingarian and Yen (1994) upon which the sulfur content of asphaltene varies from 0.3% to 10.3%. Holditch (2007) reported that oxygen exists mainly in acidic functional groups, while nitrogen atoms are present in basic functional groups. Here, though, the percentages of oxygen and nitrogen for the extracted asphaltene were 7.63% and 0.68%, respectively. It is evident that the percentage of oxygen content in comparison with nitrogen is large enough to assure the acidity of asphaltene. The small amount of oxygenated compounds would be important to determine the acidity of crude oil. This is because carboxylic acid, as an organic compound, contains oxygen which plays an important role in the acidity of crude oil.

2.3 IFT and viscosity measurements

IFT was measured by the pendant drop method using a DSA-100 apparatus. The measurements were carried out with the method presented by Alnoush *et al.* (2019). The schematic of IFT measuring set-up is illustrated in Figure 1. As in this study, the IFT of the crude oil and water was of interest then the quartz cell was filled with brine solution and the syringe with the crude oil. Then, the needle was placed inside the compartment so that it could inject the crude oil into the chamber from the bottom. The pump then slowly injected the emulsion fluid and a droplet with a volume of one microliter forms at the tip of the needle inside the quartz cell. An image was subsequently taken from the formed droplet using the camera embedded in the device. The taken image was then sent to the computer connected to the device for image analysis of the droplet. The densities of the two phases were also required to calculate the IFT of the crude oil and water which were measured and given as inputs to the software for the calculation of IFT. The repeatability error of the tests is equal to $\pm$ 0.3 mN/m.

The viscosity of W/O emulsions was measured with the method documented by Hubbard and Brown (1943) using Rolling Ball method. A ball of known dimensions rolls or falls through a closed capillary, which contains the sample liquid. A preset angle determines the inclination of the capillary. The time it takes the ball to descend a defined distance within the fluid is directly related to the fluid's viscosity. The main forces acting on the descending ball including FG (Effective portion of gravitational force), FB (Effective portion of buoyancy force) and FV (Viscous force). All experiments were performed at ambient temperature and atmospheric pressure.

2.4 Preparation of water-in-oil emulsion (static test)

Various experiments were conducted to reach the highest emulsion stability for each salt. Eleven different salt solutions in the range of 1000–100 000 ppm (*i.e.* 1000, 10 000, 20 000, 30 000, 40 000 up to 100 000 ppm) were firstly prepared with one-fifth ratio (*i.e.* 20% water and 80% oil) of water in oil emulsions. The salt solutions were then added to the spinning oil and stirred with 1000 rpm for an hour. The emulsion was subsequently poured into a test tube and was left for 2 h. A droplet of the prepared emulsion was taken from the middle of the test tube and put on the lam (*i.e.* laboratory plate) for taking images by the camera (Dino camera) with 50× zooming scale. The used camera had about 40 frame per second (fps) speed resolutions.

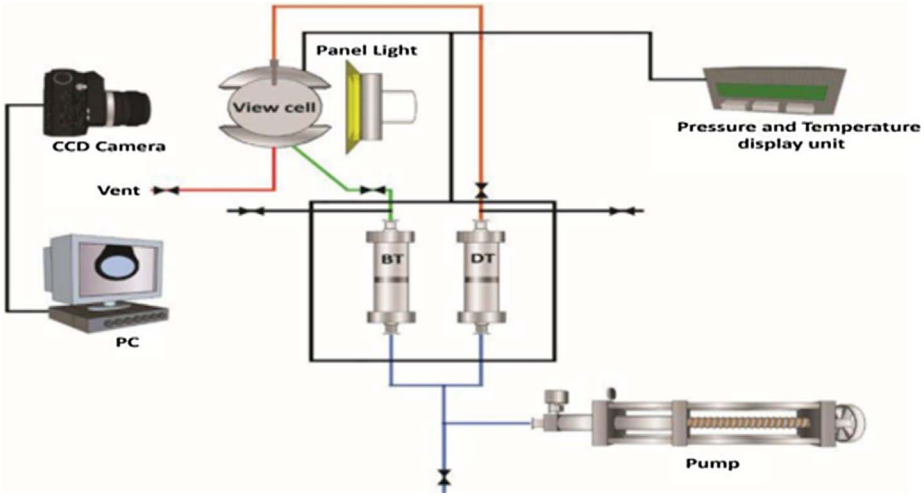

Fig. 1. Schematic view of pendant drop IFT apparatus (Ismail *et al.*, 2019).

Table 3. Geophysical characteristics of the glass micromodel.

Micromodel type	Width (cm)	Length (cm)	Pore volume (cc)	Pore diameter (μm)		
				Low permeability region	Intermediate permeability region	High permeability region
Semi-uniform pattern	6	6	0.6	200	250	350

2.5 Glass micromodel

Glass micromodel is a transparent artificial porous medium which can be used as a small-scale model of 2-D reservoir rocks. It can be used to visualize fluid flow and to understand different mechanisms and changes occurring in porous media especially those which are related to the interface of the existing phases. They are also applicable for the pore scale visualization of the particle and chemical transport in porous media. Generally, without any surface modification, micromodels are considered to be strongly water wet because they are composed of silica which is the predominant substance forming sandstones. For the construction of glass micromodels, laser technology with the acid washing was used. Initially, 39 vol% of HF acid was used to carve the flow passages. By putting another flat glass, the prepared glass micromodel was then placed in the furnace to be heated up to 750 °C. The homogeneous pattern of the micromodel was chosen in order to minimize the impact of complicated flow conditions such as the presence of tortuous fluid flow paths or dead-end pores. The micromodel also contained three distinct regions to discern the impacts of permeability on the emulsification process. The first region of the micromodel which was adjacent to its inlet was the low permeability region. The second region was of intermediate permeability and finally the third region of high permeability close to its outlet. The characteristics of the micromodel are provided in Table 3. In addition, the schematic of the micromodel geometry with different permeability regions is represented in Figure 2.

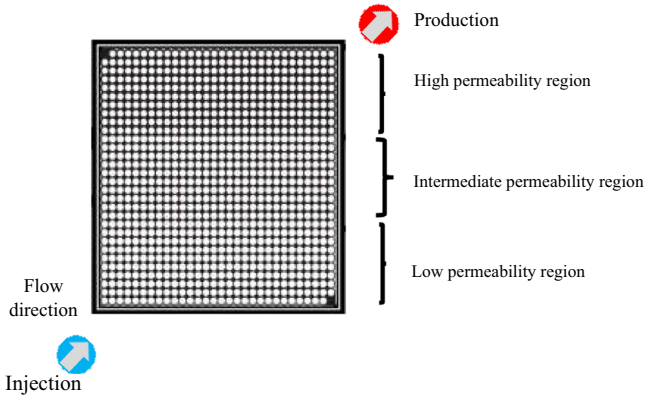

Fig. 2. Schematic of the glass micromodel.

2.6 Experimental procedure

Figure 3 shows the schematic of the experimental set-up. The precise injection of fluids into the micromodel was accomplished by the use of LA-30 syringe pump which is capable of injecting fluids with the rate up to 125 h. Using HLOT microscopic camera, fluid flow is carefully observed in micromodel. Tecl LED backlight panel was also used to enhance the quality of images and videos.

The fluids used in the experiments included crude oil, deionized water (DW), Na_2CO_3 and $MgSO_4$ brines at their optimum concentrations which were obtained from static emulsification experiments (optimum concentrations

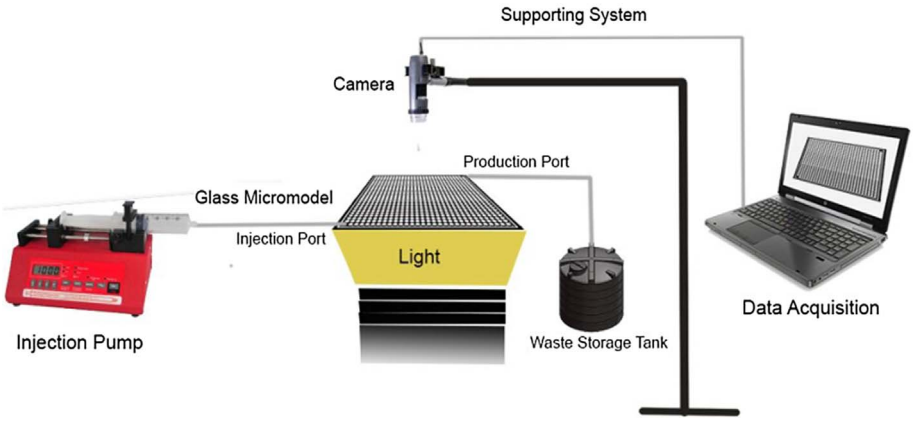

Fig. 3. Schematic of the experimental set-up.

Table 4. Detailed experimental procedure.

Experiment	Preparation procedure		First displacing fluid	Second displacing fluid
No. 1	Saturating micromodel with DW	Oil injection	DW injection (80 cc/h) (blue colored)	$MgSO_4$ brine injection (80 cc/h)
No. 2	Saturating micromodel with DW	Oil injection	DW injection (80 cc/h) (blue colored)	Na_2CO_3 brine injection (80 cc/h)
No. 3	Saturating micromodel with DW	Oil injection	DW injection (0.5 cc/h)	Na_2CO_3 brine injection (0.5 cc/h) (blue colored)

correspond to emulsions in their highest stability state). At first, DW and then crude oil were injected to the micromodel until the stable initial state was reached which was considered as the preparation procedure in Table 4. With the injection of the first displacing fluid, oil displacement process was carefully followed. Meanwhile the mechanisms through which the emulsification took place were monitored. Then with the injection of the second displacing fluid, the impacts of this second fluid on the first displacing fluid as well as its impacts on the residual oil were observed. Finally, the oil recovery factor of each process was measured and analyzed. It should be mentioned that after each experiment, the micromodel was cleaned based on the procedure reported in literature to maintain its water-wet wettability (Mehranfar and Ghazanfari, 2014).

In order to get better insight into the dynamic experiments quantitatively, an image processing algorithm (Dong *et al.*, 2006; Roman *et al.*, 2016; Zuo *et al.*, 2013) was applied using Matlab Image Processing Toolbox (*Mathworks*, 2015) and the changes in oil saturation were then tracked in the course of injection. In this analytical method, a Red, Blue and Green (RGB) color model was used and histograms of color distribution of pixels in micromodel were extracted. In the extracted histograms, the boundaries between the pixels related to each region (grains, injection fluid, and crude oil) were calibrated and the area under the distribution curve of each region was assumed as the saturation of each component in the micromodel. The used color histogram was red due to its concentration in the micromodel images. The color boundaries related to the different phases are calibrated by comparing the calculated recovery factor and the measured recovery factors before injection fluid breakthrough (recovery factor before breakthrough is easily obtained by calculating the injected volume using time and injection rate). As the calibration results depicted, the maximum error in calculated results was less than 1% of the oil saturation. Detailed information of each experiment is provided in Table 4. In addition, to confirm repeatability, all experiments were repeated three times.

3 Results and discussion

3.1 Effect of salinity on stability of emulsions at static conditions

One of the controlling parameters in the stability of the crude oil emulsions is the interactions between cations in the aqueous phase and asphaltene in the oil phase. If there is a considerable concentration of the cations in the system, they can then interact with the negatively charged asphaltene and this would, in turn, result in destabilization of the crude oil emulsions. The solubility of salts in water depends on the ionic radiuses and charges of the salt molecules. Higher solubility indicates higher ionization. The concentration of ions in the aqueous phase increases up to the saturation point. After the saturation point, further increased salt concentration resulted in the salt precipitation in the aqueous phase. Thus the number of the free ions in the

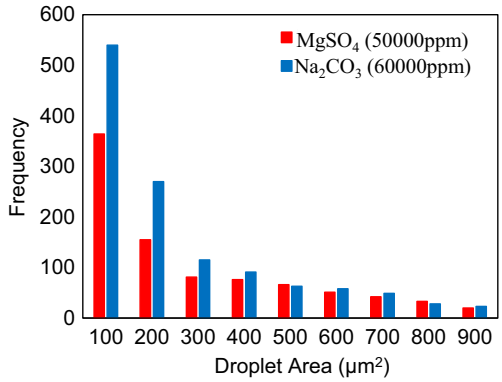

Fig. 4. Frequency of size of emulsions of 50 000 ppm $MgSO_4$ with acidic (pH = 5.6) and 60 000 ppm Na_2CO_3 basic (pH = 11.3).

Fig. 5. Images of pendant drop for measurement of IFT between the oil and aqueous solutions, (a) $MgSO_4$ solution at 50 000 ppm, (b) Na_2CO_3 solution at 60 000 ppm.

aqueous phase decreases. As it was mentioned, in this study, emulsions were stabilized using 11 different salt concentrations ranging from 1000 to 100 000 ppm. The images of emulsions were captured using light microscopy and analyzed with ImageJ as a histogram.

The optimum concentration for $MgSO_4$ was 50 000 ppm which had the highest number of dispersed area in comparison with the lower and higher concentrations. Similarly, the optimum concentration for Na_2CO_3 with the same reason was 60 000 ppm. The histograms in Figure 4 compare the number of dispersed water droplets in crude oil which were formed by $MgSO_4$ and Na_2CO_3 solutions at their optimum concentrations (in various surface areas as shown in Fig. 4). The surface area of the water droplets analyzed by the ImageJ software ranged from 100 μm^2 to 10 000 μm^2. Based on the literature (Goodarzi and Zendehboudi, 2019; Sjöblom, 2001), the more smaller surface area of dispersed water droplets, the more stable emulsions. For this reason, in this study, water droplets with the surface area ranging from 100 μm^2 to 1000 μm^2 were investigated.

Once the optimum concentration of the investigated salts had been identified, the interfacial tension between oil/$MgSO_4$ solution and oil/Na_2CO_3 solution was measured. Figure 5 shows the pendant drop of IFT analyses of the oil with different aqueous solutions. The measured IFT for oil/$MgSO_4$ solution (Fig. 5a) is 27.46 and for oil/Na_2CO_3 solution (Fig. 5b) is less than 0.01 mN/m (see Tab. 5). It is evident that the interfacial tension between the oil droplet and Na_2CO_3 solution is much lower than that for the $MgSO_4$ solution. The profound reduction of IFT should be related to reaction between the acidic components of the crude oil and the basic solution. Moreover, the considerable reduction in the interfacial tension between oil and Na_2CO_3 solution can be attributed to the produced *in-situ* surfactant (Mahdavi and Zebarjad, 2018; Sheng, 2010). As a result of this phenomenon, more water droplets with the smaller surfaces would be formed. In addition, the viscosity of emulsions was measured and reported in Table 6. As it can be seen the values for $MgSO_4$ and Na_2CO_3 are 235 cP and 512 cP, respectively.

The properties of the aqueous phases including pH and viscosity are provided in Table 5. Furthermore, the table contains the optimal concentrations of the salts and the IFT between these solutions and the crude oil.

As it can be observed from Figure 4, W/O emulsions which were produced by Na_2CO_3 solution contain the higher number of water droplets compared to that using $MgSO_4$ solution. The main reason lies in the fact that sodium carbonate had a relatively high basicity of pH = 11.3, while the measured value of pH for $MgSO_4$ solution is 5.6 which proves its acidity. Figure 5 shows the IFT for both solutions and as it can be seen, the interfacial tension between oil and Na_2CO_3 solution is much lower than that for oil and $MgSO_4$ solution. Moreover, Table 6 provides the viscosity values for emulsions. These measured values provide another evidence that the produced emulsion by Na_2CO_3 solution is tighter because of the higher number of dispersed water droplets.

3.2 Impact of high flow rate on *in-situ* emulsification and oil recovery

3.2.1 Effect of $MgSO_4$ as the second displacing fluid (No. 1)

With the rate of 80 cc/h, Deionized Water (DW) was injected to the micromodel (blue colored). The capillary number corresponding to this rate was 2.56×10^{-4} which was considerably higher than the usual capillary number taking place at the reservoir conditions. Usually, fluid flows with capillary numbers less than 10^{-5} are considered to be in reservoir regime. This flow rate generally takes place in the near wellbore region of the reservoir where higher pressure drop would serve as a driving force for the fluid flow. For such a high flow rate, emulsification would then take place as the displacing fluid (DW in this case) has a considerably high viscous force. When the water droplets collide with the grain surface then they would break up into parts forming emulsified water phase. In fact, large viscous forces are the main source of energy for the emulsification process and dispersing water droplets in crude oil medium.

Table 5. Properties of the brines and interfacial characteristics.

Fluid	Chemical formula	Optimum concentration (ppm)	pH	IFT_{wo} (mN/m)	Viscosity (cP)
Sodium carbonate	Na_2CO_3	60 000	11.3	<0.01	1.04
Magnesium sulphate Heptahydrate	$MgSO_4{\cdot}7H_2O$	50 000	5.6	27.46	1.06

Table 6. Measured viscosity of fluids at 25 °C and 1 atm.

Fluid	Viscosity (cP)
Crude oil	145
W/O emulsion using 50 000 ppm $MgSO_4$	235
W/O emulsion using 60 000 ppm Na_2SO_4	512

As injection continued, the number of dispersed water droplets in porous media increased. The driving force which was formed by the continuous displacing water phase then caused more dispersed water droplets to be collided to grains resulting in their break-up and creating more dispersed water droplets. The number of dispersed water close to the outlet of micromodel is considerably higher than that at the inlet. The likely reason is that in this region, the pressure drop was higher than the central region, which, in turn, increases the fluid velocity. Increased fluid velocity is a key factor which leads to more collision between the water droplets and grains. Consequently, the number of dispersed water droplets considerably increased (Fig. 6a).

Figure 6b represents the effects of injecting 50 000 ppm brine of $MgSO_4$ as the second displacing fluid. As it is indicated in Table 5, pH of $MgSO_4$ solution is 5.6 meaning an acidic pH. In addition to this, because of the acidic nature of crude oil (see Tab. 2) the reaction between acidic components of oil and acidic solution was not high enough to reduce the interfacial tension. Thus, this type of salt would not then noticeably be reactive with the crude oil. The interfacial tension between the fluids *i.e.* crude oil and displacing fluid is not also reduced substantially (see Fig. 5a). Thus, emulsification would not take place. Marginal reactivity with the oil phase makes the brine phase to pass through the swept region which had been previously displaced by deionized water. As a result, besides of marginal increase of oil recovery, the flow of the second displacing phase does not have any noticeable impact on the emulsification process as well as emulsion stability and displacement.

3.2.2 Effect of Na_2CO_3 as the second displacing fluid in high rate regime (No. 2)

The first part of the experiment No. 2 was similar to that of No. 1. Figure 7a shows the deionized water injection with the same flow rate (80 cc/h) as for experiment No. 1(blue colored). The primary mechanisms taking place in these two experiments were similar but for different salts. This resulted in similar patterns for the two experiments which shows good repeatability of the conducted experiments (see Fig. 8 where the oil recovery factor is similar after the first injection [water flooding] in both cases).

In this experiment, the second injected fluid was Na_2CO_3 brine with a concentration of 60 000 ppm. This salt would make the solution basic as it dissolves in water. The result would then be the reaction between the acidic components of the crude oil with the basic aqueous solution. As it is evident from Figure 7b, at first, the injected brine tended to move from the swept regions. As this phase continued to move in this region, it also detached the oil droplets which were adhered to the grain. The detachment of oil droplets can emulsify the displacing fluid and results in higher oil recovery due to the entrainment mechanism. As the injection continued (see Fig. 7c), the brine had more time to interact with the crude oil producing *in situ* surfactants. The produced surfactants then substantially decreased the interfacial tension between the displacing fluid and the crude oil (Sheng, 2010). The result of significantly low interfacial tension was the formation of emulsions. The emulsion produced in this stage of the injection caused the displacement front to be emulsified. Thus, the viscosity of the displacing fluid increased considerably which, in turn, altered the mobility ratio to a more favorable state. Consequently, the oil recovery can be increased by the W/O emulsification through the injection of the second fluid to the micromodel (see Fig. 7d).

Figure 8 shows the recovery factor of each experiment for the first and the second injection processes. As it can be seen, the oil recovery respective to the experiment No. 2 is quite higher than experiment No. 1. A possible explanation is that through this experiment, by the injection of the first fluid, crude oil is produced as the emulsification takes place. With the injection of the second fluid, reaction between the acidic components of the crude oil and the basic solution new emulsions would then be produced. This new emulsification process increased the oil recovery which, in turn, made this scenario more effective than experiment No. 1. Finally Figure 8 reaffirms that the scenario of injecting brine as the second displacing fluid yielded higher oil recovery factor as much as 53%. The interaction between the brine and the crude oil was the main reason for such a profound difference.

3.3 Impact of reservoir capillary dominant flow rate on *in-situ* emulsification and oil recovery

For low flow injection rates, capillary force is dominant and the viscous force of the injected fluid is much less than the case of high flow rate injection. In these experiments, the flow rate was 0.5 cc/h and the respective capillary number

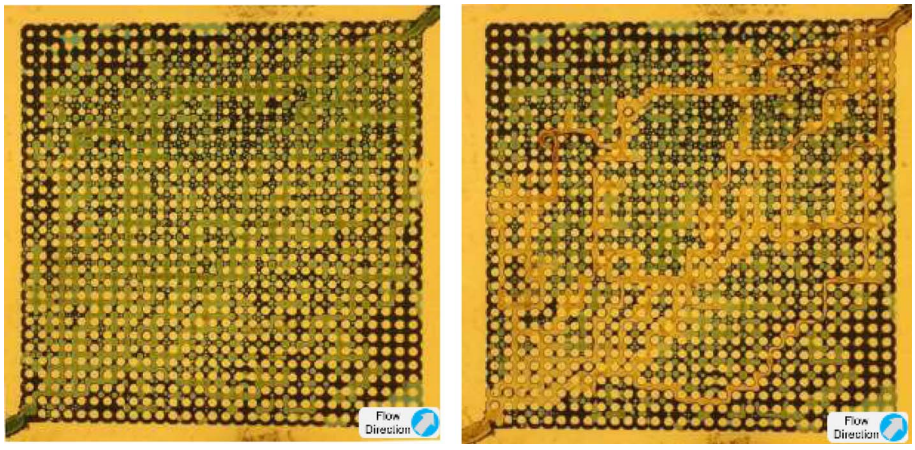

Fig. 6. Emulsion patterns (a) after 3 PV of blue colored deionized water injection; (b) after 3.3 PV of $MgSO_4$ brine injection.

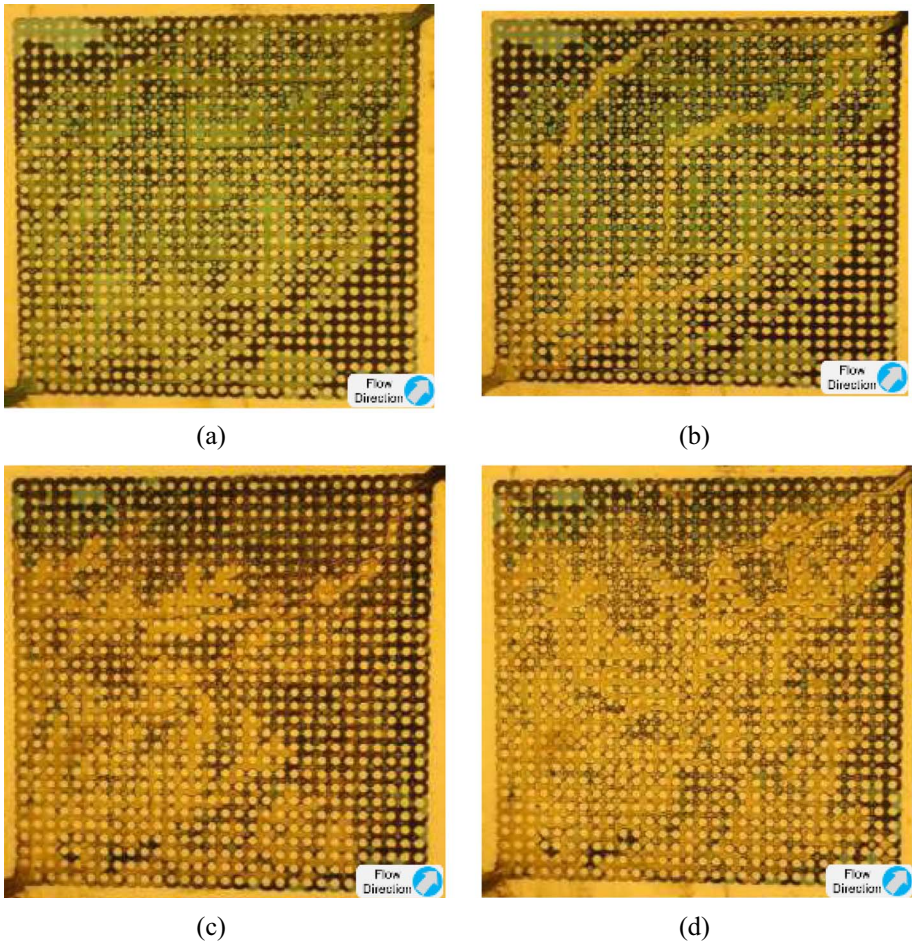

Fig. 7. Impact of Na_2CO_3 brine injection (a) initial state after 3 PV blue colored deionized water injection; (b) after 1.6 PV of Na_2CO_3 brine injection; (c) after 2.1 PV of Na_2CO_3 brine injection; (d) after 3.3 PV of Na_2CO_3 brine injection.

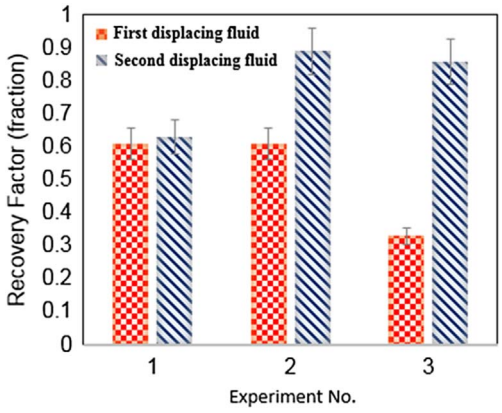

Fig. 8. Oil recovery for experiments No. 1 (High rate DW and $MgSO_4$), No. 2 (High rate DW and Na_2CO_3) and No. 3 (Low rate DW and Na_2CO_3) (see Tab. 4 for details).

equaled to 1.6×10^{-6} which was quite similar to the capillary number occurring at the reservoir conditions. The injected fluid had more time to react with the crude oil components. In this section, experiment No. 2 was repeated but with the lower flow rate resembling those in the reservoir. This new experiment is referenced as experiment No. 3. Since the flow rate was low, then the basic injected fluid had more time to interact with acidic components of the oil phase. As a result, more *in-situ* surfactants were expected to be produced in the light of reduced IFT between the displaced and displacing fluid (Fig. 5b). Emulsification process then would inevitably be enhanced and wettability alteration mechanisms would be more probable to occur (Palizdan *et al.*, 2020). Lower flow rates also reduced the viscous force in comparison with the higher flow rates. As the viscous force of the displacing fluid reduces, the extent of viscous fingering process which is an adverse phenomenon for the oil recovery would be decreased. Thus,

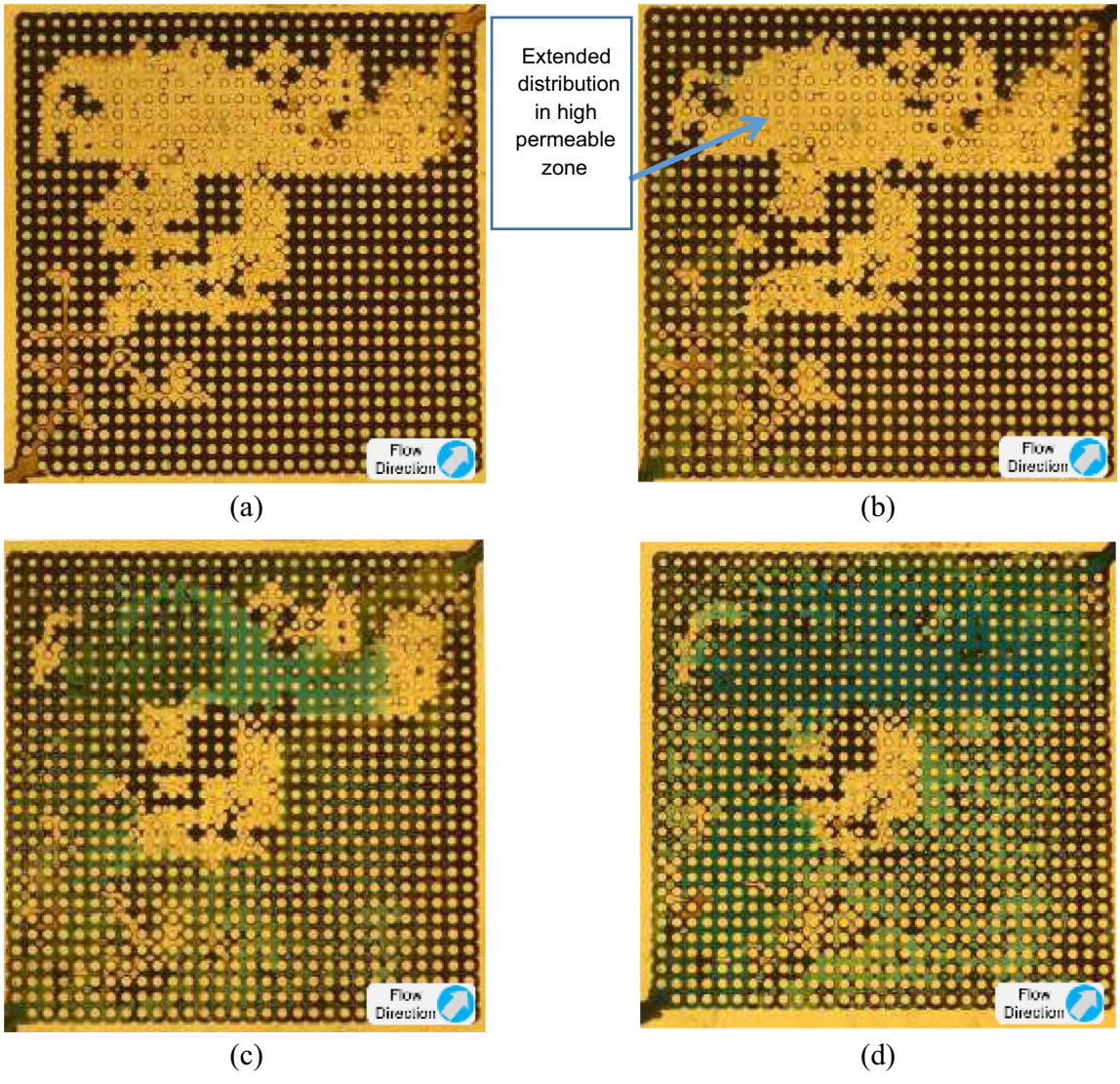

Fig. 9. Flow pattern of low flow rate (0.5 cc/h) (a) after 1 PV deionized water flooding (b) after 0.16 PV of blue colored Na_2CO_3 brine injection; (c) after 0.5 PV of blue colored Na_2CO_3 brine injection; (d) after 1.25 PV of blue colored Na_2CO_3 brine injection.

higher oil recovery and sweep efficiency are expected during the low flow rate injection process. Moreover, in the course of capillary dominant flow, different permeability regions of the micromodel were more distinguishable compared to that of the viscous dominant flow.

3.3.1 Effect of Na_2CO_3 as the second displacing fluid at low flow rates (No. 3)

Figure 9 shows the injection of displacing fluids with the rate of 0.5 cc/h into the glass micromodel. The respective capillary number is 1.6×10^{-6} which was quite close to the capillary number at the reservoir condition. At first, deionized water was injected to the micromodel. As the injected fluid penetrated into the micromodel, it preferred to flow in two different directions. One was the direction of the pressure gradient which was along the entrance of the micromodel to its exit. The second preferred flow direction, was the direction towards the regions with higher permeability. Since in such regions, the resistance towards the flow was less than the lower permeable regions, then the fluid preferentially passed through the direction of the higher permeability. With the injection of the second fluid (blue colored), as it was already mentioned, the brine interacted with the un-swept crude oil to create *in situ* surfactants forming W/O emulsions (see Fig. 9a). The reduction in the IFT not only caused the displacing fluid to be emulsified, but also increased the microscopic displacement efficiency. Thus, that portion of the oil can be produced which was trapped in small pores. As it was stated earlier, emulsification can increase the viscosity of the displacing fluid (see Tab. 6). As the viscosity of the displacing fluid increased further, the emulsified front would displace oil in more piston-wise manner which means higher macroscopic sweep efficiency. It can be seen from Figure 9b that by continuing the injection, the injected fluid preferred to pass through the regions where less resistance existed towards its flow. Consequently, the produced emulsions and injected fluid would rather flow in the direction of the swept regions. Figure 9c also demonstrates that in some spots, the oil film which surrounded the dispersed water droplets prevented the emulsion to be fully miscible with the deionized water present in the swept region. Thus, water in the swept spots deviated the flow direction of the emulsion. This deviation increased the oil recovery since the emulsion passed through other un-swept regions rather than the previously swept regions. High permeable regions are more favorable for the emulsions to flow through. As a result, an extended distribution for the emulsions, as for the deionized water, can be visualized in high permeable regions (see Fig. 9d).

4 Conclusion

The results obtained in this study highlighted the importance of the scenarios which may be followed during reservoir production. It should be mentioned that at reservoir scale, different factors including the heterogeneity in the pore space and differences in the types of the formation water may also play role in the stability of the emulsified phase. Further studies, including core flooding experiments and up-scaled reservoir simulation studies would also help to consolidate the findings of the present study. The following conclusions can be drawn from the results of present experimental study in which different solutions of Na_2CO_3 and $MgSO_4$ with various flow rates were injected into the micromodel in different injection orders:

- By increase of the salt solubility and its ability to release free anions and cations, the likely interactions between polar parts of the crude oil (*i.e.* asphaltene) and the free ions of the solution were enhanced and the number of dispersed water droplets in oil increased causing much higher viscosity of the formed *in-situ* emulsion.
- The intensity of emulsification close to the micromodel exit was greater likely due to the higher pressure drop and fluid flow driving force.
- Due to the high basicity of Na_2CO_3 brine, it started to interact with the acidic components of the crude oil as it came into contact with the crude oil. This, in turn, reduced the IFT to profoundly low values.
- The injection of the Na_2CO_3 brine emulsified the displacing front causing higher viscosity. The mobility ratio was then reduced thus larger oil recovery would be expected.
- Oil recovery was substantially improved when alkaline solution injected after deionized water. This was mainly due to the fact that the injection of basic brine to the micromodel caused further *in-situ* emulsification.

Acknowledgments. The authors would like to thank the valuable advice and help of EOR Research Centre personnel including Sanaz Shojaei, Zahra Etemadan, Jassem Abbasi and Hamid Taghavinejad. The financial and technical supports of *South Zagros Oil and Gas Production Company* (*SZOGPC*) and *Petroazma Company* would also be acknowledged.

References

Akizuki Y., Yoshida M., Ishida N., Oshiki T., Oshitani J. (2014) PH Effect on properties of surfactant-free oil-in-water emulsion prepared with oleic acid. *Chem. Lett.* **43**, 5, 604–606.

Alnoush W., Sayed A., Alyafei N. (2019) Optimization of contact angle and interfacial tension measurements for fluid/rock systems at ambient conditions, *MethodsX* **6**, March, 1706–1715.

Alvarado D.A. (1979) *Flow of oil-in-water emulsions through tubes and porous media (December)*, Society of Petroleum Engineers.

Bryan J., Kantzas A. (2007) *SPE 110738, Enhanced Heavy-Oil Recovery by Alkali-Surfactant Flooding"*, Society of Petroleum Engineers. http://www.spe.org/elibrary/servlet/spepreview?id=SPE-110738-MS.

Bryan J., Mai A., Kantzas A. (2008) Investigation into the processes responsible for heavy oil recovery by alkali-surfactant flooding, in: *SPE – DOE Improved Oil Recovery Symposium Proceedings*, pp. 1–13. https://doi.org/10.2118/113993-MS

Chilingarian G.V., Yen T.F. (1994) *Asphaltenes and asphalts*, Elsevier, p. 1.

Dong M., Qiang L., Aifen L. (2007) Micromodel study of the displacement mechanisms of enhanced heavy oil recovery, in: *Presentation at the International Symposium of the Society of Core Analysts held in Calgary, Canada, 10–12 September*, pp. 1–6.

Dong W., David Suits L., Sheahan T.C., Selvadurai A.P.S. (2006) Image Processing Technique for Determining the Concentration of a Chemical in a Fluid-Saturated Porous Medium, *Geotechnical Testing Journal* **29**, 5, 100024.

Doryani H., Seyede E.B., Masoud R., Mohammad R.M. (2017) Experimental investigation of alkali flooding on enhanced recovery of an asphaltenic oil, *Pet. Res.* **27**, 107–121.

Farias M., Carvalho M., Souza A., Hirasaki G., Miller C. (2012) A comparative study of emulsion flooding and other IOR methods for heavy oil fields, *Society of Petroleum Engineers*. https://doi.org/10.2118/152290-MS.

Feng H., Kang W., Zhang L., Chen J., Li Z., Zhou Q., Wua H. (2018) Experimental study on a fine emulsion flooding system to enhance oil recovery for low permeability reservoirs, *J. Pet. Sci. Eng.* **171**, 974–981. https://doi.org/10.1016/j.petrol.2018.08.011.

Goodarzi F., Zendehboudi S. (2019) A comprehensive review on emulsions and emulsion stability in chemical and energy industries, *Canadian J. Chem. Eng.* **97**, 1, 281–309.

Holditch S.A. (2007) *IV: Operations petroleum engineering production operations engineering*, Society of Petroleum Engineers.

Hubbard R.M., Brown G.G. (1943) The rolling ball viscometer, *Indus. Eng. Chem. – Anal. Edn.* **15**, 3, 212–218.

Ismail I., Kazemzadeh Y., Sharifi M., Riazi M., Malayeri M.R., Cortés F. (2019) Formation and stability of W/O emulsions in presence of asphaltene at reservoir thermodynamic conditions, *J. Mol. Liq.* **299**, 112125. https://doi.org/10.1016/j.molliq.2019.112125.

Karambeigi M.S., Abbassi R., Roayaei E., Emadi M.A. (2015) Emulsion flooding for enhanced oil recovery: interactive optimization of phase behavior, microvisual and core-flood experiments, *J. Indus. Eng. Chem.* **29**, 382–391. https://doi.org/10.1016/j.jiec.2015.04.019.

Kazemzadeh Y., Ismail I., Rezvani H., Sharifi M., Riazi M. (2019) Experimental investigation of stability of water in oil emulsions at reservoir conditions: effect of ion type, ion concentration, and system pressure, *Fuel* **243**, 15–27.

Kumar R., Dao E.K., Mohanty K.K. (2010) Emulsion flooding of heavy oil, in: *SPE Improved Oil Recovery Symposium*, Society of Petroleum Engineers.

Liu Q., Dong M., Yue X., Hou J. (2006) Synergy of alkali and surfactant in emulsification of heavy oil in brine, *Colloids Surf. A: Physicochem. Eng. Aspects* **273**, 1–3, 219–228.

Mahdavi E., Zebarjad F.S. (2018) Fundamentals of enhanced oil and gas recovery from conventional and unconventional reservoirs, in: *Screening Criteria of Enhanced Oil Recovery Methods*, Elsevier Inc. https://doi.org/10.1016/B978-0-12-813027-8.00002-3.

Mai A., Kantzas A. (2009) Heavy oil waterflooding: effects of flow rate and oil viscosity, *J. Canadian Pet. Technol.* **48**, 3, 42–51.

Mathworks (2015) *Mathworks MATLAB Manual 2015*, R2015b.

Mehranfar A., Ghazanfari M.H. (2014) Investigation of the microscopic displacement mechanisms and macroscopic behavior of alkaline flooding at different wettability conditions in shaly glass micromodels, *J. Pet. Sci. Eng.* **122**, 595–615. https://doi.org/10.1016/j.petrol.2014.08.027.

Palizdan S., Abbasi J., Riazi M., Malayeri M.R. (2020) Impact of solutal Marangoni convection on oil recovery during chemical flooding, *Pet. Sci.* **17**, 1298–1317. https://doi.org/10.1007/s12182-020-00451-z.

Pei H., Zhang G., Ge J., Ma M., Zhang L., Liu Y.L. (2013a) Improvement of sweep efficiency by alkaline flooding for heavy oil reservoirs, *J. Disp. Sci. Technol.* **34**, 11, 1548–1556. https://doi.org/10.1080/01932691.2012.752331.

Pei H., Zhang G., Ge J., Jin L., Ma C. (2013b) Potential of alkaline flooding to enhance heavy oil recovery through water-in-oil emulsification, *Fuel* **104**, 284–293. https://doi.org/10.1016/j.fuel.2012.08.024.

Poteau S., Argillier J.F., Langevin D., Pincet F. (2005) Influence of PH on stability and dynamic properties of asphaltenes and other amphiphilic molecules at the oil-water interface, *Energy Fuels* **19**, 4, 1337–1341.

Pu W., Shen C., Tang X., Pang S., Sun D., Mei Z. (2019) Emulsification of acidic heavy oil for viscosity reduction and enhanced oil recovery, *J. Disp. Sci. Technol.* **41**, 54–61. https://doi.org/10.1080/01932691.2018.1544908.

Rezaei N., Firoozabadi A. (2014) Macro- and microscale waterflooding performances of crudes which form w/o emulsions upon mixing with brines, *Energy Fuels* **28**, 3, 2092–2103.

Roman S., Soulaine C., AlSaud M.A., Kovscek A., Tchelepi H. (2016) Particle velocimetry analysis of immiscible two-phase flow in micromodels, *Adv. Water Res.* **95**, 199–211.

Rudin J., Bernard C., Wasan D.T. (1994), Effect of added surfactant on interfacial tension and spontaneous emulsification in alkali/acidic oil systems, *Indus. Eng. Chem. Res.* **33**, 1150–1158.

Sabooniha E., Rokhforouz M.R., Ayatollahi S. (2019) Pore-scale investigation of selective plugging mechanism in immiscible two-phase flow using phase-field method, *Oil Gas Sci. Technol. - Rev. IFP Energies nouvelles* **74**, 78. https://doi.org/10.2516/ogst/2019050.

Saha R., Uppaluri R., Tiwari P. (2018) Influence of emulsification, interfacial tension, wettability alteration and saponification on residual oil recovery by alkali flooding, *J. Indus. Eng. Chem.* **59**, October, 286–296. https://doi.org/10.1016/j.jiec.2017.10.034.

Schmidt D.P., Soo H., Radke C.J. (1984) *Linear oil displacement by the emulsion entrapment process*, Society of Petroleum Engineers, pp. 351–360.

Shahsavani B., Malayeri M.R., Riazi M. (2019) Impact of aqueous phase in emulsified form on distribution and instability of asphaltene molecules, *J. Mol. Liq.* **295**, 111688. https://doi.org/10.1016/j.molliq.2019.111688.

Shang X., Bai Y., Sun J., Dong C. (2019) Performance and displacement mechanism of a surfactant/compound alkaline flooding system for enhanced oil recovery, *Colloids Surf. A: Physicochem. Eng. Aspects* **580**, July, 123679. https://doi.org/10.1016/j.colsurfa.2019.123679.

Sheng J. (2010) *Modern chemical enhanced oil recovery: theory and practice*, Gulf Professional Publishing.

Sheng J.J. (2015) Status of alkalinesurfactant flooding, *Polym. Sci.* **1**, 1.

Sjöblom J. (Hrsg.) (2001) *Encyclopedic Handbook of Emulsion Technology*, http://login.ezproxy.library.ualberta.ca/login?url=http://search.ebscohost.com/login.aspx?direct=true&db=edscea&AN=EDSCEA.CEAB20021100230&site=eds-live&scope=site.

Soo H., Radke C.J. (1984) Velocity effects in emulsion flow through porous media, *J. Colloid Interface Sci.* **102**, 2, 462–476.

Soot H., Radke C.J. (1984) Flow mechanism of dilute, stable emulsions in porous media, *Indus. Eng. Chem. Fundam.* **23**, 342–347.

Sun J.H., Zhang F.S., Wu Y.W., Liu G.L., Li X.N., Su H.M., Zhu Z.Y. (2019) Overview of emulsified viscosity reducer for enhancing heavy oil recovery, *IOP Conf. Ser. Mater. Sci. Eng.* **479**, 012009.

Taiwo O.A., Mamudu A., Dagogo-Jack C., Joshua D., Olafuyi O. (2016) *Grain Size Effects on Residual Oil Saturation*, Society of Petroleum Engineers. https://doi.org/10.2118/184296-MS.

Thomas S. (2008) Enhanced oil recovery – an overview, *Oil Gas Sci. Technol. - Rev. IFP Energies nouvelles* **63**, 1, 9–19.

Umar A.A., Saaid I.B.M., Sulaimon A.A., Pilus R.B.M. (2018) A review of petroleum emulsions and recent progress on water-in-crude oil emulsions stabilized by natural surfactants and solids, *J. Pet. Sci. Eng.* **165**, 673–690. https://doi.org/10.1016/j.petrol.2018.03.014.

Wang J., Dong M. (2009) *Simulation of O/W emulsion flow in alkaline/surfactant flood for heavy oil recovery*, Petroleum Society of Canada, pp. 1–13.

Wang J., Dong M., Arhuoma M. (2010) Experimental and numerical study of improving heavy oil recovery by alkaline flooding in sandpacks, *J/ Canadian Pet. Technol.* **49**, 3, 51–57.

Youssef S., Rosenberg E., Deschamps H., Oughanem R., Maire E., Mokso R. (2014) Oil ganglia dynamics in natural porous media during surfactant flooding captured by ultra-fast X-ray microtomography, in: *International Symposium of the Society of Core Analysts (SCA2014-023)*, pp. 1–12.

Zuo L., Zhang C., Falta R.W., Benson S.M. (2013) Micromodel investigations of CO_2 exsolution from carbonated water in sedimentary rocks, *Adv. Water Resour.* **53**, 188–197.